PNAS

Supplementary Information for

Anthropogenic drivers of 2013–2017 trends in summer surface ozone in China

Ke Li[a,b], Daniel J. Jacob[b,1], Hong Liao[a,c,1], Lu Shen[b], Qiang Zhang[d], and Kelvin H. Bates[b]

[a]Harvard-NUIST Joint Laboratory for Air Quality and Climate, Nanjing University of Information Science and Technology, Nanjing 210044, China

[b]John A. Paulson School of Engineering and Applied Sciences, Harvard University, Cambridge, MA 02138, United States

[c]Jiangsu Key Laboratory of Atmospheric Environment Monitoring and Pollution Control, Collaborative Innovation Center of Atmospheric Environment and Equipment Technology, School of Environmental Science and Engineering, Nanjing University of Information Science & Technology, Nanjing 210044, China

[d]Department of Earth System Science, Tsinghua University, Beijing 100084, China

[1]*Correspondence to*:
Email: Daniel J. Jacob (djacob@fas.harvard.edu) or Hong Liao (hongliao@nuist.edu.cn)

This PDF file includes:
    Supplementary text
    Figs. S1 to S9
    Tables S1 to S4
    Reference

Supplementary Information Text

1 GEOS-Chem simulations

1.1 Detailed GEOS-Chem description

The simulations of tropospheric ozone were carried out with the nested-grid version of the GEOS-Chem model with a horizontal resolution of 0.5° × 0.625° (version 11-02, http://geos-chem.org) (1), driven by the assimilated meteorological data of MERRA-2. The nested domain is set over Asia (60°–150°E, 10°S–55°N), and chemical boundary conditions are updated every 3 h from a global simulation with 4° × 5° resolution. The GEOS-Chem model includes fully coupled ozone-NO_x-VOC-halogen-aerosol chemistry (2) with up-to-date chemical rate constants from JPL Publication 15-10. The impact of aerosols on gas-phase chemistry in GEOS-Chem is through the effect of aerosol extinction on photolysis rates (3) and through heterogeneous processes (4). Heterogeneous processes include N_2O_5 uptake by aerosols from Evans and Jacob (5), the absorption of NO_3 and NO_2 on wet aerosols (4), and HO_2 uptake with a reactive uptake coefficient of 0.2 for conversion to H_2O (4, 6).

Emissions in GEOS-Chem model are computed by the Harvard-NASA Emission Component (HEMCO), as introduced by Keller et al. (7). Global default anthropogenic emissions are from the CEDS (Community Emissions Data System, 8). They are overwritten by MEIC (Multi-resolution Emission Inventory for China) in China and by MIX in other regions of Asia (9). Open fire emissions are from the Global Fire Emissions Database (GFED4) (10). Natural emissions of ozone precursors, including NO_x from lighting and soil and VOCs from vegetation, are calculated on the basis of the assimilated MERRA-2 meteorology. The biogenic emissions of VOC are calculated according to the Model of Emissions of Gases and Aerosols from Nature (MEGAN-2; 11).

1.2 Evaluation of GEOS-Chem simulation

The capability of the GEOS-Chem model to simulate surface ozone over China has been evaluated using ground-level measurements (12–14), aircraft (15,16), ozonesonde data (16), and satellites (17). Here we evaluate the GEOS-Chem simulation with the China Ministry of Ecology and Environment (MEE) surface measurement network used in this work. Fig. S2 shows the comparison for 2017. MDA8 ozone over China has an average value of 58.5±15.4 ppb in the observations and 63.0±14.8 ppbv in the model. The spatial pattern of summertime ozone is well captured, with a correlation coefficient of 0.89. For $PM_{2.5}$, observed and simulated values have an average of 27.2±10.8, and 28.7±16.8 μg m^{-3}, respectively, with a correlation coefficient of 0.70.

1.3 Sensitivity simulations

To identify the driving factors of the ozone trend, we performed a set of sensitivity simulations using the GEOS-Chem model (**Table S4**). We conducted a control run simulation with 2013 MEIC emissions and 2013 MERRA-2 meteorology (CTRL) and a set of sensitivity runs:

(1) The same as the CTRL simulation except Chinese anthropogenic NO_x and VOC emissions are set to 2017. (Run_NO_x_VOC);

(2) The same as the CTRL simulation except Chinese anthropogenic NO_x emissions are set to 2017 (Run_NO_x);

(3) The same as the CTRL simulation except simulated aerosol extinction (AOD) is scaled to 2017 using satellite-based AOD changes in the calculation of photolysis rates and simulated aerosol surface area is scaled to 2017 using measurement-based $PM_{2.5}$ changes in the calculation of heterogeneous reactions (Run_Hete_All);

(4) The same as the Run_Hete_All simulation except measurement-based $PM_{2.5}$ changes are not applied in the calculation of aerosol chemistry reactions for N_2O_5 (Run_Hete_N_2O_5);

(5) The same as the Run_Hete_All simulation except measurement-based $PM_{2.5}$ changes are not applied in the calculation of aerosol chemistry reactions for NO_2/NO_3 (Run_Hete_NO_x);

(6) The same as the Run_Hete_All simulation except measurement-based $PM_{2.5}$ changes are not applied in the calculation of aerosol chemistry reactions for HO_2 (Run_Hete_HO_2);

(7) The same as the CTRL simulation except simulated aerosol extinction (AOD) is scaled to 2017 using satellite-based AOD changes in the calculation of photolysis rates and (Run_AOD).

(8) The same as the Run_Hete_HO_2 simulation except product of HO_2 uptake by aerosol changed from H_2O to H_2O_2. (Run_Hete_HO_2_H_2O_2).

The effect of aerosol chemistry in the sensitivity simulation is estimated using changes in measured $PM_{2.5}$ concentrations from 2013 to 2017 that are applied as scaling factors to simulated aerosol surface area in the boundary layer below 1.3 km. The effect of changing AOD on photolysis rates is estimated using observed changes in AOD from 2013 to 2017 applied as scaling factors to simulated AOD in the calculation of photolysis rate through the tropospheric column. All simulations were performed for the period of 1 June to 31 August of meteorological year 2013 after a one-month model spin up.

2 Attribution of anthropogenic drivers in ozone trend

The roles of changing emissions of ozone precursors (NO_x and VOC) are quantified by simulations of Run_NO_x_VOC and Run_NO_x. The role of aerosol chemistry is estimated by

3

simulations of Run_Hete_All, Run_Hete_N$_2$O$_5$, Run_Hete_NO$_x$, and Run_Hete_HO$_2$. The effect of aerosols on photolysis rates is estimated by Run_AOD. **Fig. S7** shows the measured and simulated 2013–2017 anthropogenic trends (ppbv a^{-1}) for the representative cities in the four focus megacity clusters, including the effects from individual model processes. The observed trends are for the residuals after removing the effect of meteorological variability (**Fig. 3**), and are for a single 0.5° × 0.625° grid cell representative of the urban core (to avoid averaging effects between grid cells).
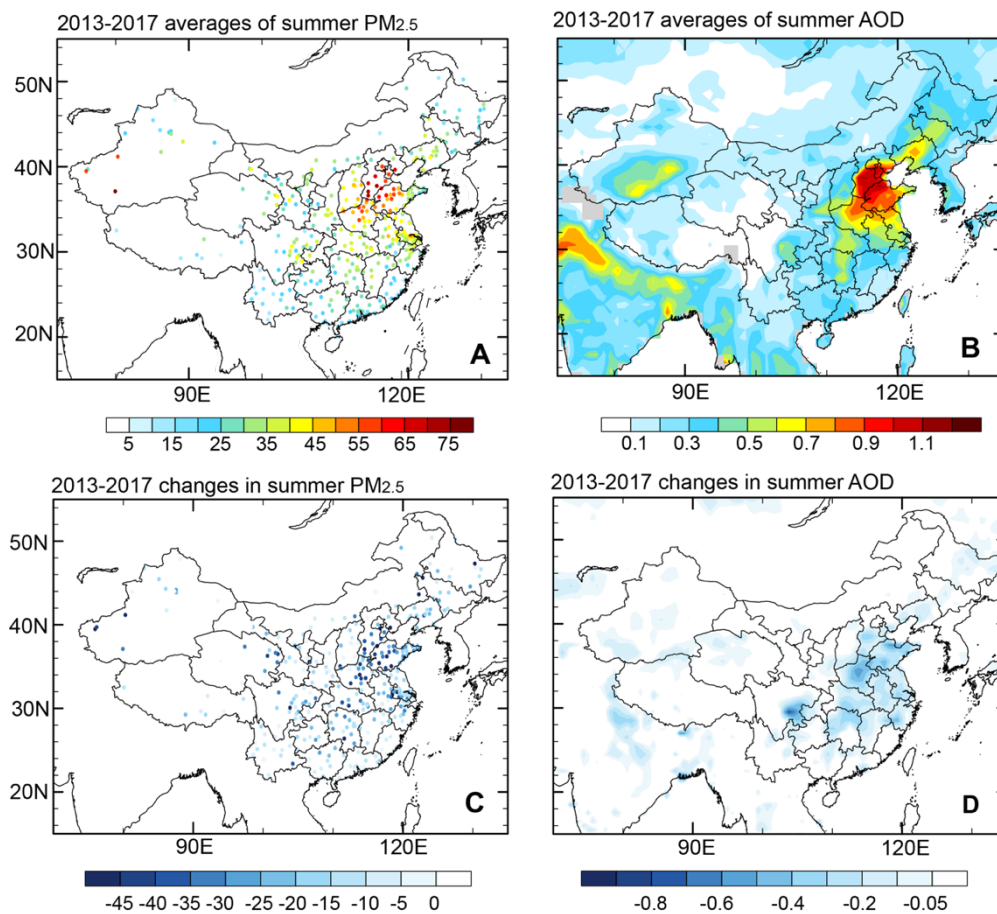
Fig. S1. *Top*: summer mean PM$_{2.5}$ concentrations (µg m^{-3}) (**A**) and MODIS aerosol optical depth (AOD) (**B**) during 2013–2017. *Bottom*: changes in summer mean PM$_{2.5}$ concentrations (µg m^{-3}) (**C**) and MODIS aerosol optical depth (AOD) (**D**) from 2013 to 2017. Changes in PM$_{2.5}$ concentrations are applied to aerosol surface area in the lower atmosphere (1st-10th model level, i.e., below 1.3 km) in the calculation of heterogeneous reactions by aerosols. Changes in AOD are applied to the calculation of photolysis rate through tropospheric column. Hourly surface PM$_{2.5}$ concentrations for 2013–2017 were obtained from the MEE surface observation network. The MODIS AOD is based on the monthly level-3 product (MYD08_M3) from the Aqua satellite at 550 nm with a resolution of 1° × 1°.

5
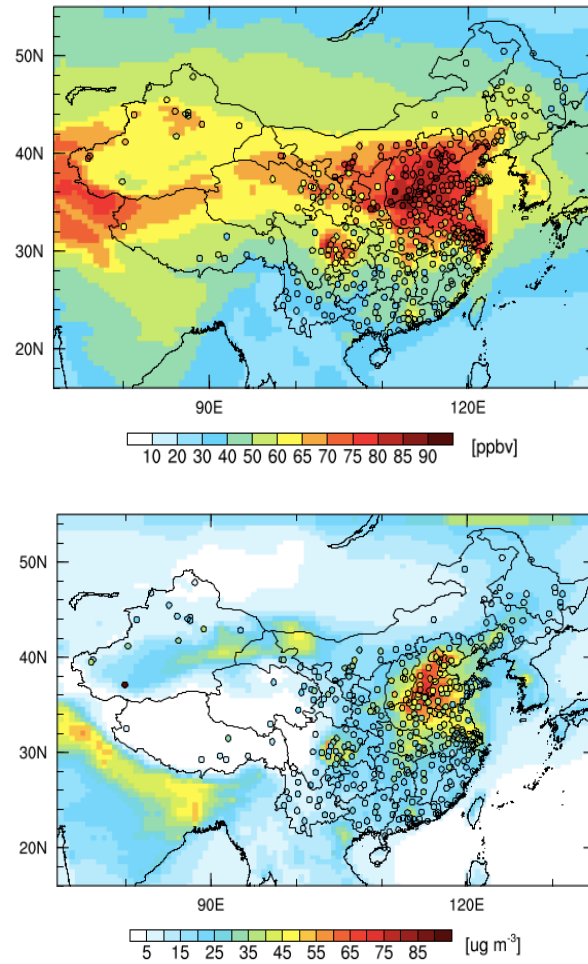
Fig. S2. Comparison of simulated (contour) and observed (dotted) MDA8 ozone (***top***) and PM$_{2.5}$ (***bottom***) in summer of 2017. The observed and simulated ozone concentration have an average of 58.5±15.4 and 63.0±14.8 ppbv, respectively, and a correlation coefficient of 0.89. For PM$_{2.5}$, observed and simulated values have an average of 27.2±10.8, and 28.7±16.8 μg m^{-3}, respectively, and a correlation coefficient of 0.70.
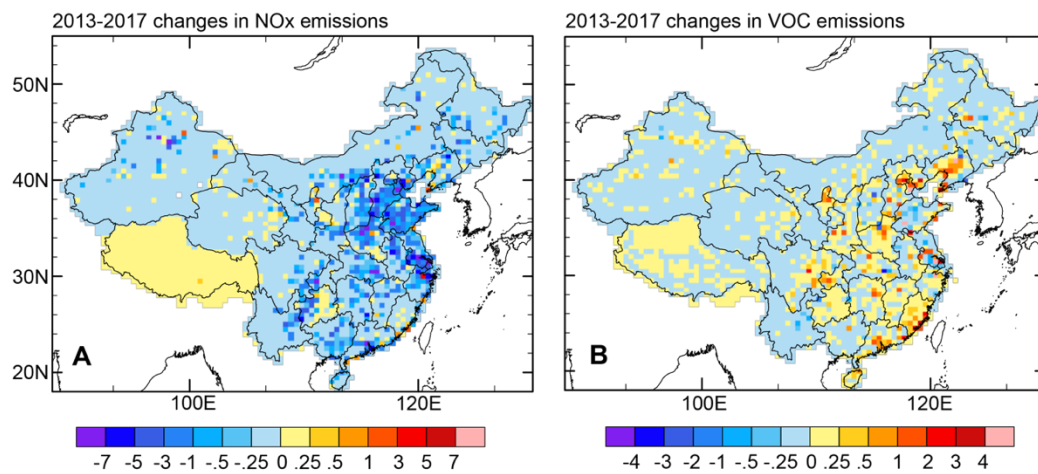
Fig. S3. 2013–2017 changes in anthropogenic emissions estimated from the MEIC inventory. Changes of NO_x emissions (Gg NO_x/grid cell) (**A**) and VOC emissions (Gg C/grid cell) (**B**) in summer between 2017 and 2013. The grid cells are 0.5° × 0.666°.
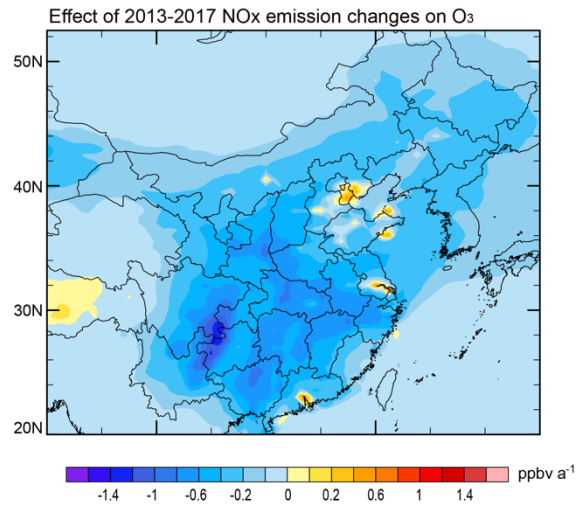
Fig. S4. Effects of 2013–2017 anthropogenic NO_x emission changes on summer MDA8 ozone. The Figure shows GEOS-Chem model results for the changes in MDA8 ozone resulting from 2013–2017 changes in NO_x emissions alone.
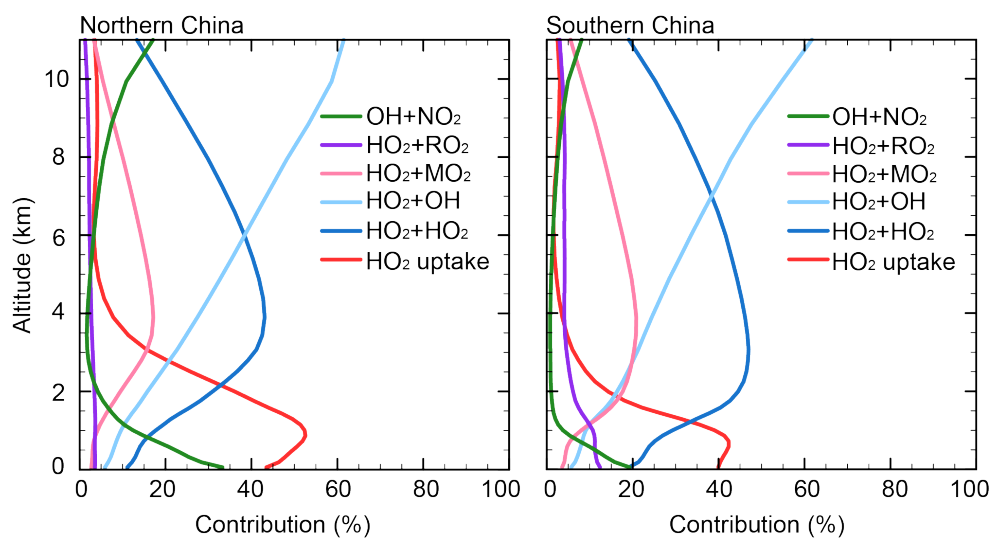
Fig. S5. GEOS-Chem simulated relative contributions of major loss pathways to the total HO_x sink over northern China (100°–120°E, 34°–42°N, ***left***) and southern China (100°–120°E, 22°–30°N, ***right***) in summer 2016. MO_2 refers to the methylperoxy radical (CH_3O_2) and RO_2 refers to all other organic peroxy radicals.

Sensitivity of ozone to product of HO_2 uptake by aerosols

HO_2 uptake product: H_2O HO_2 uptake product: H_2O_2
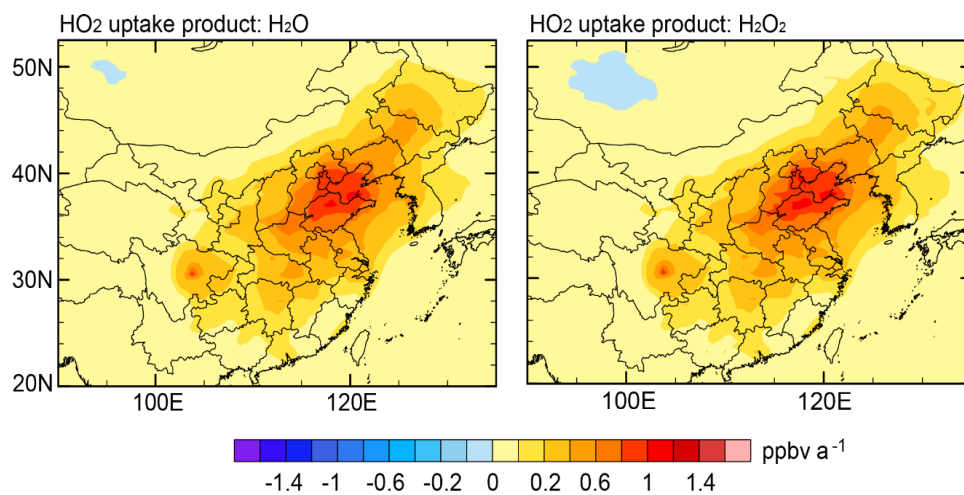
Fig. S6. Simulated effects on mean summer MDA8 ozone when the product of HO_2 uptake by aerosols is taken to be H_2O (*left*) or H_2O_2 (*right*), as determined by difference between corresponding GEOS-Chem simulations for 2013 (see **Table S4**).
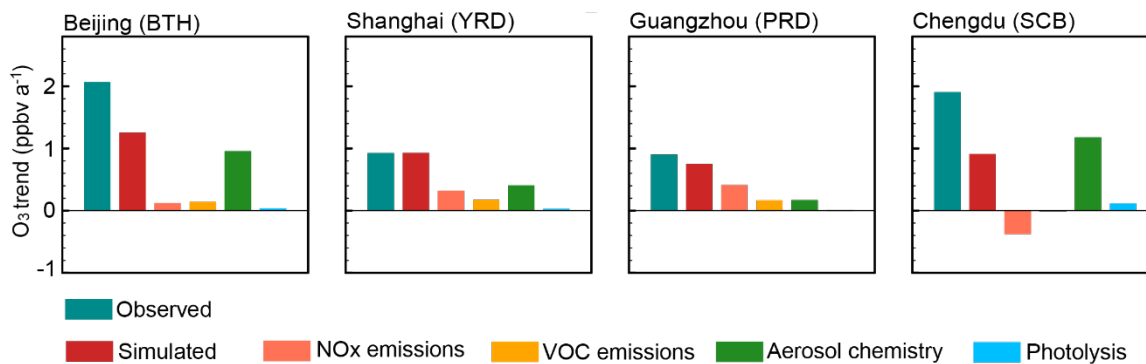
Fig. S7. Measured and simulated 2013–2017 anthropogenic ozone trends (ppbv a^{-1}) for representative cities in the four focus megacity clusters, including the effects from individual model processes. The observed trends are for the residuals after removing the effect of meteorological variability (**Fig. 3**), and for single 0.5° × 0.625° grid cells in the urban core.

Tmax_corr(Obs,MERRA2)   RH_corr(Obs,MERRA2)

0.1 0.2 0.3 0.4 0.5 0.6 0.7 0.8 0.9
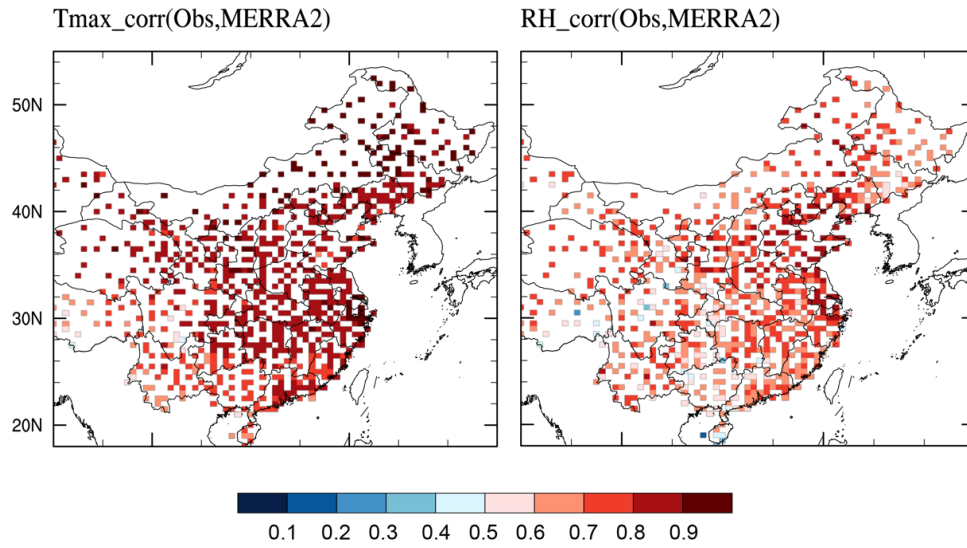
Fig. S8. Correlation coefficients between MERRA-2 and weather station measurements of daily maximum temperature (Tmax, ***left***) and daily mean relative humidity (RH, ***right***) during the 2013–2017 summers. A total of 839 Chinese weather stations with continuous records from the China National Meteorological Information Center (NMIC; http://data.cma.cn/en) are used, with data averaged onto the 0.5° latitude × 0.625° longitude MERRA-2 grid.
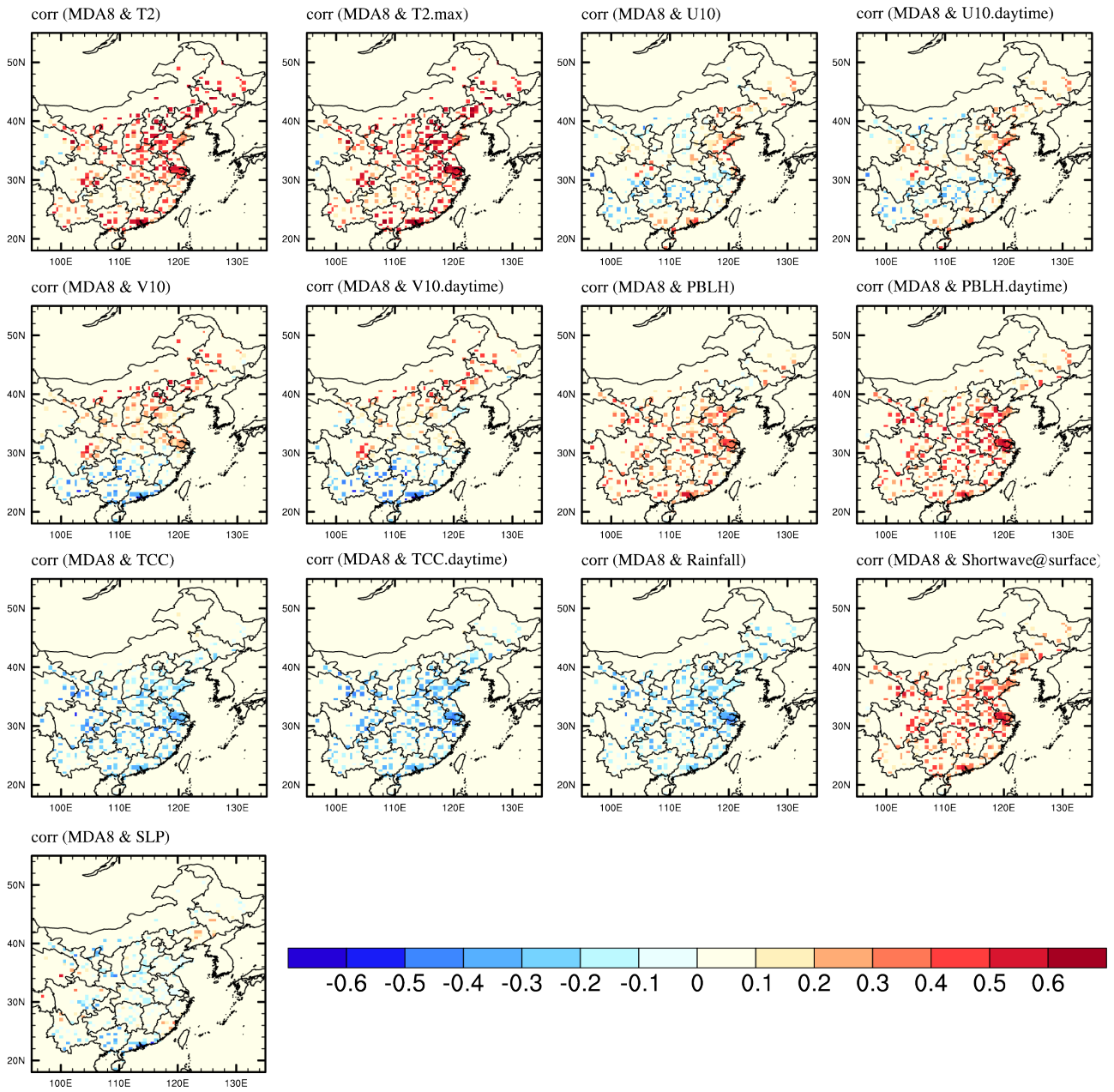
Fig. S9. Correlation coefficients of daily MDA8 ozone and meteorological variables for 2013–2017 summers. Only correlation coefficients that are statistically significant at 95% confidence level are shown. See details for variables in **Table S3**.

Fig. S9. Continued.

14
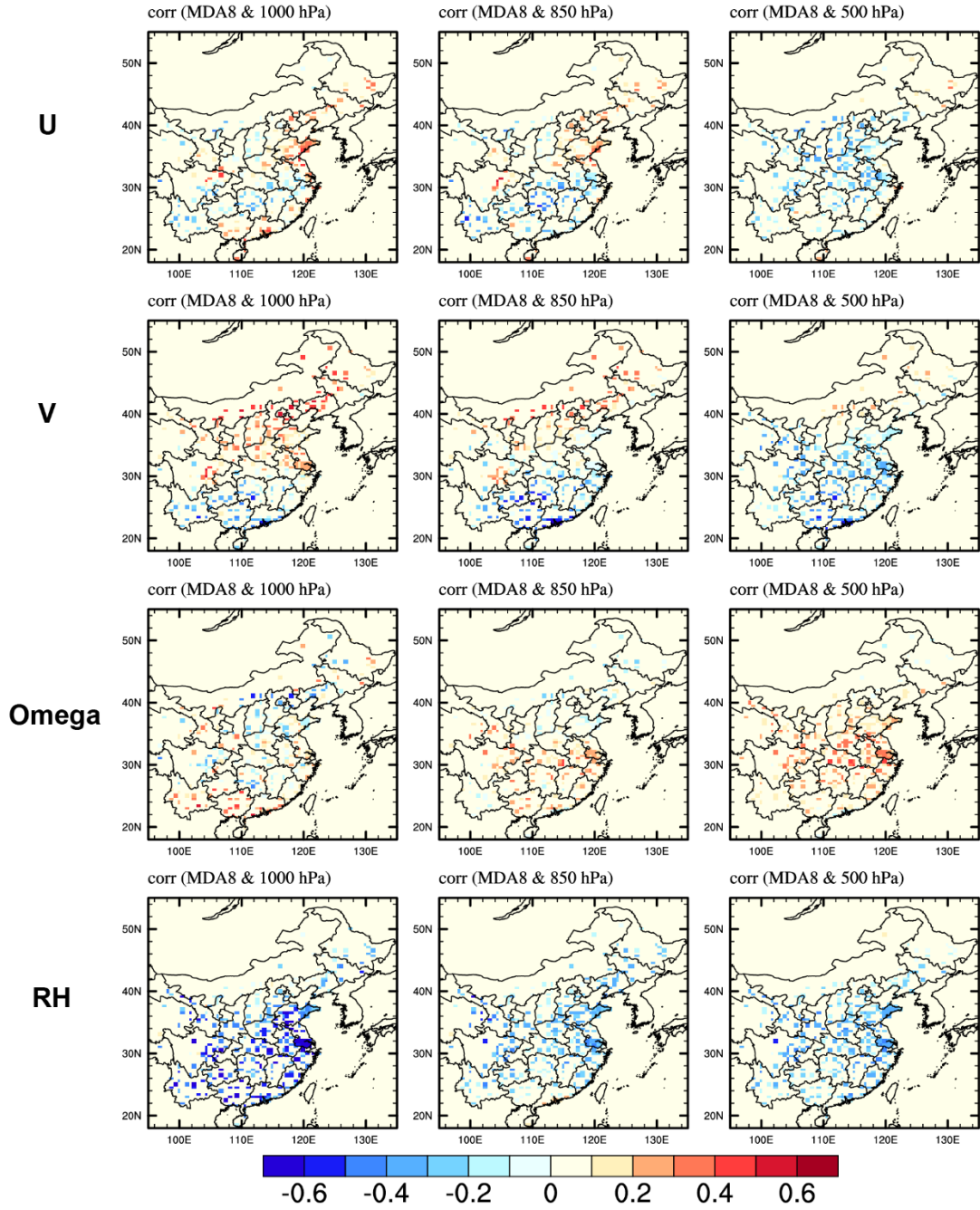
Table S1. **Statistics for observed ozone trends (ppbv a^{-1}) during 2013–2017[a].**

Region	number of sites	Average	Median	Maximum	Minimum
BTH	13	3.11	2.97	5.25	0.20
YRD	22	2.29	1.64	10.2	-2.88
PRD	12	0.56	0.74	3.99	-1.82
SCB	14	1.63	1.25	6.72	-0.65

[a] Trends for the ensemble of sites in the four megacity clusters of **Fig. 1**.

Table S2. **Percentage changes (%) of emissions and PM$_{2.5}$ concentrations from 2013 to 2017.**[a]

Region	NO$_x$	VOC	SO$_2$	OC	BC	PM$_{2.5}$
BTH	−23	+6.7	−66	−46	−39	−41
YRD	−21	+8.2	−67	−35	−26	−36
PRD	−16	+3.7	−45	−32	−19	−12
SCB	−17	+5.8	−67	−32	−31	−39
China	−21	+2.0	−59	−32	−28	−40

[a]Anthropogenic emission trends of NO$_x$, VOC, SO$_2$, organic carbon aerosol (OC), and black carbon aerosol (BC) are estimated from the MEIC inventory (18). PM$_{2.5}$ trends from the MEE surface observation network.

Table S3. **Meteorological fields considered as possible ozone covariates.**

MERRA-2 surface variables[a]		MERRA-2 surface variables[a]	
Acronym	Description	Acronym	Description
T2	2-m air temperature (K)	PBLH.daytime	planetary boundary layer height averaged over 08:00 to 16:00 LT (m)
Tmax	daily maximum 2-m air temperature (K)	TCC	total cloud area fraction (100%)
U10	10-m zonal wind (m s^{-1})	TCC.daytime	total cloud area fraction averaged over 08:00 to 16:00 LT (%)
U10.daytime	10-m zonal wind averaged over 08:00 to 16:00 LT (m s^{-1})	Rainfall	total precipitation (mm d^{-1})
V10	10-m meridional wind (m s^{-1})	SLP	sea level pressure (Pa)
V10.daytime	10-m zonal wind averaged over 08:00 to 16:00 LT (m s^{-1})	Shortwave@surface	surface incoming shortwave flux (W m^{-2})
PBLH	planetary boundary layer height (m)		
MERRA-2 variables at pressure level (1000 hPa, 850 hPa, and 500 hPa)[b]			
U	zonal wind (m s^{-1})	Omega	vertical pressure velocity (Pa s^{-1})
V	meridional wind (m s^{-1})	RH	relative humidity (100%)

[a]Temporal resolution is one-hour.
[b]Temporal resolution is three-hour.

Table S4. **GEOS-Chem sensitivity simulations**

Simulation	NO_x	VOC	Aerosol chemistry	Photolysis rates
CTRL	2013	2013	YES	YES
Run_NO_x_VOC	2017	2017	same as CTRL	same as CTRL
Run_NO_x	2017	2013	same as CTRL	same as CTRL
Run_Hete_All	2013	2013	scaled by $PM_{2.5}$ changes for all aerosol chemistry	scaled by AOD change
Run_Hete_N_2O_5	2013	2013	scaled by $PM_{2.5}$ changes only for NO_2/NO_3 and HO_2	scaled by AOD change
Run_Hete_NO_x	2013	2013	scaled by $PM_{2.5}$ changes only for N_2O_5/HO_2	scaled by AOD change
Run_Hete_HO_2	2013	2013	scaled by $PM_{2.5}$ changes only for $N_2O_5/NO_2/NO_3$	scaled by AOD change
Run_AOD	2013	2013	same as CTRL	scaled by AOD change
Run_Hete_HO_2_H_2O_2	2013	2013	same as Run_Hete_HO_2 but with H_2O_2 being HO_2 uptake product	scaled by AOD change

References

1. Chen D, et al. (2009) Regional CO pollution and export in China simulated by the high-resolution nested-grid GEOS-Chem model. *Atmos Chem Phys* 9:3825-3839.
2. Sherwen T, et al. (2016) Global impacts of tropospheric halogens (Cl, Br, I) on oxidants and composition in GEOS-Chem. *Atmos Chem Phys* 16:12239-12271.
3. Martin RV, Jacob DJ, Yantosca RM, Chin M, Ginoux P (2003) Global and regional decreases in tropospheric oxidants from photochemical effects of aerosols. *J Geophy Res* 108:4097.
4. Jacob DJ (2000) Heterogeneous chemistry and tropospheric ozone. *Atmos Environ* 34:2131-2159.
5. Evans MJ, Jacob DJ (2005) Impact of new laboratory studies of N2O5 hydrolysis on global model budgets of tropospheric nitrogen oxides, ozone, and OH. *Geophys Res Lett* 32:L09813.
6. Mao J, Fan S, Jacob DJ, Travis KR (2013) Radical loss in the atmosphere from Cu-Fe redox coupling in aerosols. *Atmos Chem Phys* 13:509-519.
7. Keller CA, et al. (2014) HEMCO v1.0: a versatile, ESMF-compliant component for calculating emissions in atmospheric models. *Geoscientific Model Development,* 7: 1409-1417.
8. Hoesly RM, et al. (2018) Historical (1750–2014) anthropogenic emissions of reactive gases and aerosols from the Community Emissions Data System (CEDS). *Geoscientific Model Development,* 11:369-408.
9. Li M, et al. (2017) MIX: a mosaic Asian anthropogenic emission inventory under the international collaboration framework of the MICS-Asia and HTAP. *Atmos Chem Phys* 17:935-963.
10. van der Werf GR, et al. (2010) Global fire emissions and the contribution of deforestation, savanna, forest, agricultural, and peat fires (1997–2009). *Atmos Chem Phys* 10:11707-11735.
11. Guenther A, et al. (2006) Estimates of global terrestrial isoprene emissions using MEGAN (Model of Emissions of Gases and Aerosols from Nature). *Atmos Chem Phys* 6:3181-3210.
12. Lou S, Liao H, Zhu B (2014) Impacts of aerosols on surface-layer ozone concentrations in China through heterogeneous reactions and changes in photolysis rates. *Atmos Environ* 85:123-138.
13. Zhu J, Liao H (2016) Future ozone air quality and radiative forcing over China owing to future changes in emissions under the Representative Concentration Pathways (RCPs). *J Geophy Res* 121:1978-2001.
14. Zhu J, Liao H, Mao Y, Yang Y, Jiang H (2017) Interannual variation, decadal trend, and future change in ozone outflow from East Asia. *Atmos Chem Phys* 17:3729-3747.
15. Wang Y, Zhang Y, Hao J, Luo M (2011) Seasonal and spatial variability of surface ozone over China: contributions from background and domestic pollution. *Atmos Chem Phys* 11:3511-3525.
16. Ni R, Lin J, Yan Y, Lin W (2018) Foreign and domestic contributions to springtime ozone over China. *Atmos Chem Phys* 18:11447-11469.
17. Wang Y, et al. (2013) Sensitivity of surface ozone over China to 2000–2050 global changes of climate and emissions. *Atmos Environ* 75:374-382.
18. Zheng B, et al. (2018) Trends in China's anthropogenic emissions since 2010 as the consequence of clean air actions. *Atmos Chem Phys* 18:14095-14111.